Materials Science-Poland, 32(1), 2014, pp. 16-22
http://www.materialsscience.pwr.wroc.pl/
DOI: 10.2478/s13536-013-0150-4

VERSITA

Effect of temperature on the electrical properties of $Zn_{0.95}M_{0.05}O$ (M = Zn, Fe, Ni)

A. SEDKY[1,2*], S. B. MOHAMED[1]

[1]Physics Department, Faculty of Science, Assiut University, Assiut, Egypt
[2]Physics Department, Faculty of Science, King Faisal University, Al-Hassa 31982, P.O.B 400, Saudi Arabia

We report here the structural and electrical properties of $Zn_{0.95}M_{0.05}O$ ceramic varistors, M = Zn, Ni and Fe. The samples were tested for phase purity and structural morphology by using X-Ray diffraction XRD and scanning electron microscope SEM techniques. The current-voltage characteristics J-E were obtained by dc electrical measurements in the temperature range of 300 – 500 K. Addition of doping did not influence the hexagonal wurtzite structure of ZnO ceramics. Furthermore, the lattice parameters ratio c/a for hexagonal distortion and the length of the bond parallel to the c axis, u were nearly unaffected. The average grain size was decreased from 1.57 μm for ZnO to 1.19 μm for Ni sample and to 1.22 μm for Fe sample. The breakdown field E_B was decreased as the temperature increased, in the following order: Fe > Zn > Ni. The nonlinear region was clearly observed for all samples as the temperature increased up to 400 K and completely disappeared with further increase of temperature up to 500 K. The values of nonlinear coefficient, α were between 1.16 and 42 for all samples, in the following order: Fe > Zn > Ni. Moreover, the electrical conductivity σ was gradually increased as the temperature increased up to 500 K, in the following order: Ni > Zn > Fe. On the other hand, the activation energies were 0.194 eV, 0.136 and 0.223 eV for all samples, in the following order: Fe, Zn and Ni. These results have been discussed in terms of valence states, magnetic moment and thermo-ionic emission, which were produced by the doping, and controlling the potential barrier of ZnO.

Keywords: *ceramics; chemical synthesis; X-Ray diffraction; electrical properties*

1. Introduction

Zinc oxide varistor is a ceramic semiconductor device with nonlinear current-voltage characteristics. An increase in applied voltage causes a decrease of resistance, and therefore the current increases strongly. This nonlinear characteristics is symmetrical and it is the same for both voltage polarities [1]. A typical ZnO based varistor is a very complex chemical system and it contains several oxide dopants such as Bi_2O_3, Cr_2O_3, Al_2O_3 , MnO, CoO, and Fe_2O_3 [2–5]. The nonlinear current-voltage characteristics of ZnO varistors are directly dependent on the composition and microstructure such as density, phase purity, grain size and structural morphology.

It is well known that the charge transfer controls the electrical conduction in ZnO varistors during sintering in oxidizing atmosphere [6–9]. The existence of potential barriers across the grain boundaries of ZnO is confirmed by the voltage contrast imaging in the scanning electron microscope (SEM) [10]. However, the energy gap E_g = 3.2 eV and the exciton binding energy = 60 meV for ZnO [11]. At low applied fields, the barrier height slightly decreases with the applied field because the electrons capture some excess of the negative interface charge, above their absolute value, which normally prevents the sharp barrier lowering. On the other hand, at high field (≈3.2 V) per grain boundary, the barrier height is reduced more significantly due to decreasing the negative interface charge below the absolute value as a result of holes creation. The appearance of positive charge at low fields can lead to a strong increase of the leakage current and helps to explain nonlinear behavior of ZnO varistors [2]. However, the impact of ionization in the depletion region of the grains of ZnO can give a

*E-mail: sedky1960@yahoo.com

sharp decrease of the barrier height even in the case of thermionic emission [12]. For this purpose, in this work a range of ZnO ceramic $Zn_{0.95}M_{0.05}O$ samples with different magnetic ions additives at Zn sites such as M = Zn, Fe, Ni were synthesized and tested by XRD and SEM techniques. The J-E characteristics were measured at different temperatures up to 500 K. Furthermore, the electrical conductivity and the activation energies at the considered temperatures were determined.

2. Experimental details

$Zn_{0.95}M_{0.05}O$ samples with M = Zn, Ni, and Fe were synthesized by using conventional solid-state reaction method. The powders of ZnO, Fe_2O_3 and NiO (Aldrich 99.999 purity) were thoroughly mixed in required proportions and calcined at 1000 °C in air for a period of 12 hours. The resulting powders were ground, mixed, and pressed into pellets of 1 cm diameter and 0. 35 cm thickness. The pellets were then sintered at temperature of 1000 °C for 10 h in air, and then quenched down to room temperature. The bulk density of the samples was measured in terms of their weight and volume. The phase purity of the samples was examined by using X-Ray diffractometer with Cu–Kα radiation. The J-E characteristics were obtained by using dc electrical circuit with an electrometer (model 6517, Keithley), dc power supply (5 kV), temperature controller and digital multimeter. The samples were well polished and sandwiched between two copper electrodes and the current was measured relative to the applied voltage at different values of temperatures (300 – 500 K). From the values of currents and voltage, the values of current density J and electric field E were obtained.

3. Results and discussion

The bulk density of ZnO, listed in Table 1, decreases with the doping. It is generally changed to 90 % for Ni and to 87 % for Fe as compared to the density of ZnO. It is evident from the XRD pattern, shown in Fig. 1, that the structure of all samples is of wurtzite type, and the other reacted phases are not formed. The obtained peaks (100), (002), (111), (102), (110), (103), (200), (112), (201), (210) and (211), shown in the XRD patterns can be identified as the hexagonal wurtzite structure of ZnO. To further confirm that the dopant has been substituted for Zn^{2+} in the unit cell, the lattice parameters were calculated and listed in Table 1. The change in lattice parameters with the Ni and Fe increase, is probably due to the difference in ionic size of doping (Ni^{2+} = 0.69 Å and $Fe^{2+/3+}$ = 0.78 Å) in comparison to Zn^{2+} (0.74 Å). However, in a real ZnO crystal, the wurtzite structure deviates from the ideal arrangement by changing the c/a ratio for hexagonal distortion or the u value for the length of the bond parallel to the c axis, in the units of c. u = 0.333 $(a/c)^2$+ 0.25 [13], and it is generally equal to 0.375 in an ideal wurtzite structure in fractional coordinates. The values of a/c ratio and u parameter shown in Table 1 are nearly unaffected by the doping. The values of a/c ratio are 0.622, 0.620 and 0.624, and the values of u parameter are 0.379, 0.378 and 0.380 for Zn, Ni and Fe, respectively. However, the deviation from the ideal wurtzite structure has not been obtained in the present case due to the lattice stability and iconicity [14]. The microstructure of the samples is shown in Fig. 2 (a – c). Although no second phases have been formed by the doping at the grain boundaries, the average grain size is decreased as compared to ZnO sample. The flake type grains are absent in all samples, and there is a uniform granular precipitation on the mother grains. The average crystalline diameters listed in Table 1 are decreased from 1.57 μm for ZnO to 1.19 μm and 1.22 μm for Ni and Fe samples, respectively. The average grain size is in the following order: Zn > Fe > Ni.

Fig. 3 (a – c) shows the J-E characteristics for all samples at the considered temperatures (300 K, 350 K, 400 K, 450 K and 500 K). It is evident that the behavior of J-E curves is ohmic in the low field region and nonohmic in the high field regions. The J-E curves are gradually shifted to lower values of the applied fields as the temperature increases up to 500 K. The upturn region is clearly observed for all samples as the temperature increases up to 400 K, and it completely disappears with further increase of temperature up to 500 K. However, the breakdown field E_B is usually taken as the field

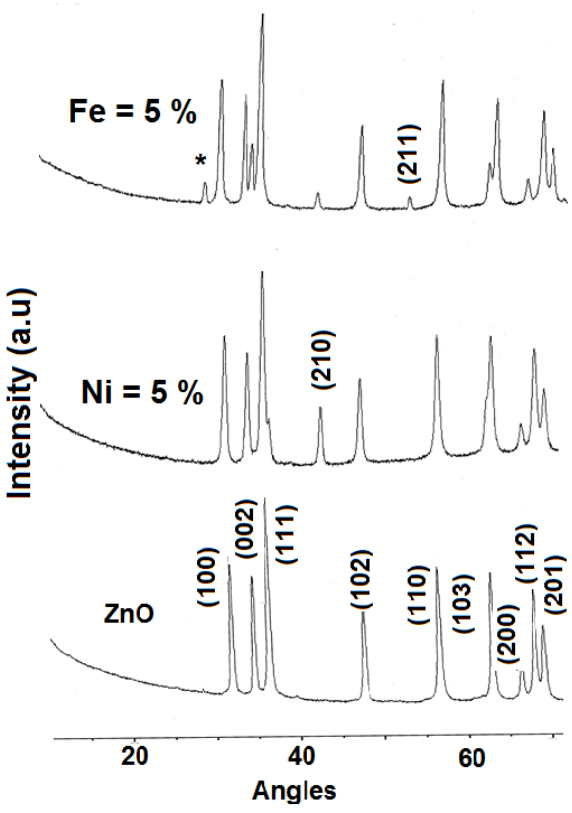

Fig. 1. XRD patterns of $Zn_{0.95}M_{0.05}O$ samples.

Table 1. Bulk density, lattice parameters, a/c ratio, u parameter, grain size and activation energy for $Zn_{0.95}M_{0.05}O$ samples with different doping elements.

Al content	ρ (g/cm^3)	**a** (Å)	**c** (Å)	**a/c**	**U** (V)	**D** (µm)	**E_a** (eV)
Zn	4.82	3.243	5.211	0.622	0.379	1.57	0.194
Fe	4.17	3.257	5.217	0.624	0.380	1.22	0.223
Ni	4.36	3.225	5.198	0.620	0.378	1.19	0.138

when the current flowing through the varistor is 1 mA/cm^2 [15–17]. The variation of E_B against temperature for all samples is shown in Fig. 4 (a) and the detailed values of E_B are listed in Table 2. It is clear that E_B decreases as the temperature increases, and it is between 25.8 V/cm and 500 V/cm for all the samples. The change in E_B values with the doping is in the following order: Fe > Zn > Ni.

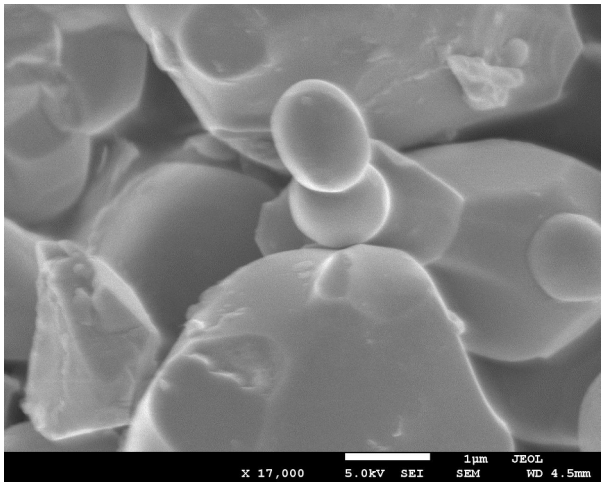

(a)

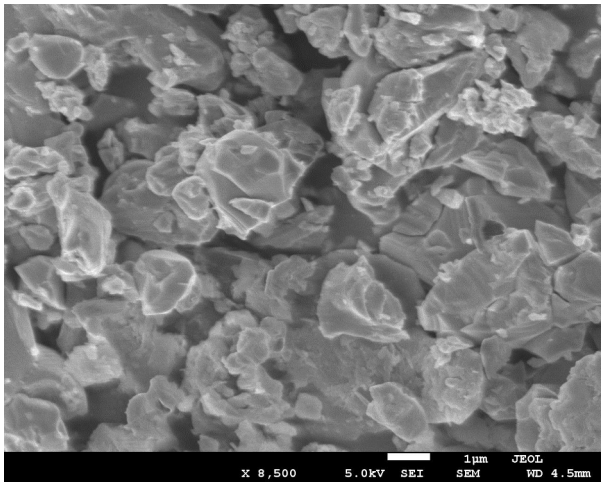

(b)

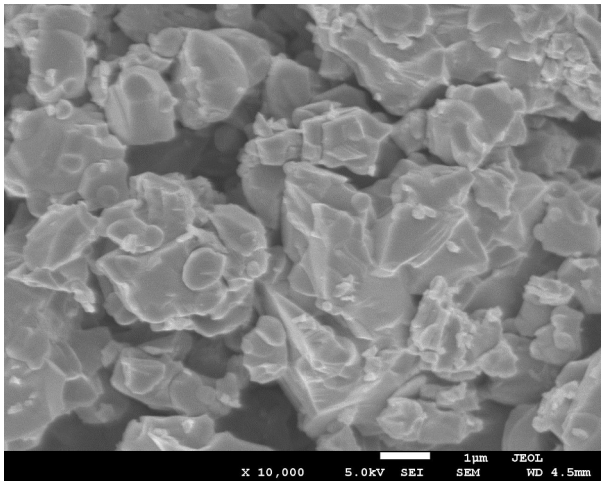

(c)

Fig. 2. SEM micrographs for (a) ZnO, (b) $Zn_{0.95}Fe_{0.05}O$ and (c) $Zn_{0.95}Ni_{0.05}O$ samples.

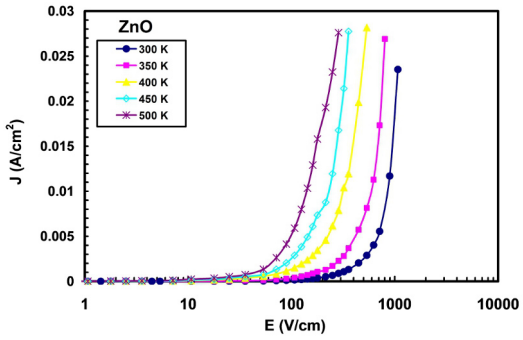

(a)

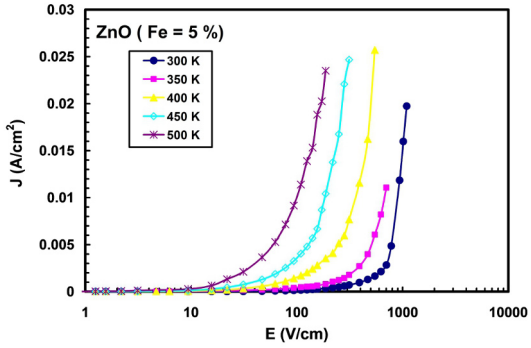

(b)

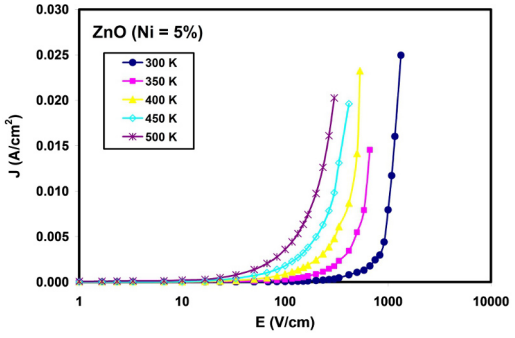

(c)

Fig. 3. J-E curves (a) ZnO, (b) $Zn_{0.95}Fe_{0.05}O$ and (c) $Zn_{0.95}Ni_{0.05}O$ samples.

The current-voltage relation of a varistor is given by the following equation [16, 17]:

$$J = \left(\frac{E}{C}\right)^{\alpha} \tag{1}$$

where J is the current density, E is the applied electric field, C is a proportionality constant corresponding to the resistance of ohmic resistor (nonlinear resistance) and α is the nonlinear coefficient.

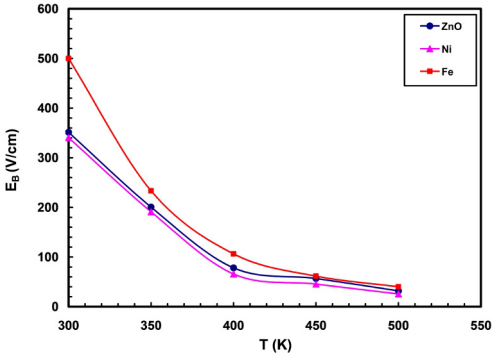

(a)

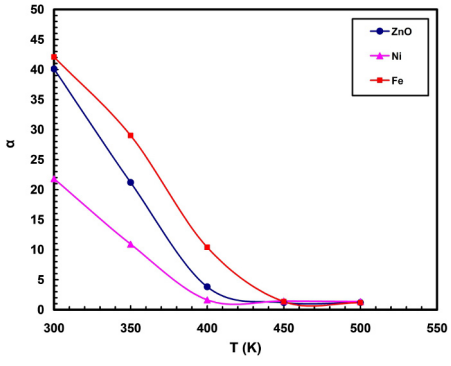

(b)

Fig. 4. Breakdown field E_B (a) and nonlinear coefficient α (b), versus temperature for $Zn_{0.95}M_{0.05}O$ samples.

Table 2. Breakdown field E_B and nonlinear coefficient α versus temperature for $Zn_{0.95}M_{0.05}O$ samples with different doping elements.

T (K)	E_B Zn (V/cm)	E_B Ni (V/cm)	E_B Fe (V/cm)	α Zn	α Ni	α Fe
300	351.4	340.6	500	40.1	21.82	42
350	200.6	191.2	233.3	21.2	10.92	29
400	78.1	65.8	106.3	3.82	1.64	10.4
450	56.7	45.7	61.7	1.18	1.45	1.36
500	31.9	25.8	40.2	1.2	1.35	1.16

The current-voltage curves are plotted on a log-log scale, from which the slope of the curve gives the value of α [18]. The variation of α against temperature in the three different regions is shown in Fig. 4 (b) whereas the detailed values are given

in Table 2. It is apparent that the α coefficient is changing up to temperature of 400 K, and it stabilizes with further increase of temperature up to 500 K. The values of α are between 1.16 and 42 for all the samples, in the following order: Fe $>$ Zn $>$ Co. These results indicate that the increase of temperature up to 400 K deforms the non ohmic features and shifts the breakdown fields to the lower values, as reported in [19].

The electrical conductivity σ against temperature for all samples can be calculated from the (J/E) in the ohmic range, considering the currents and voltages are distributed uniformly over the cross-section and thickness of the samples. However, in the second region (nonlinear region), the current strongly increases due to the decrease of potential barrier height φ_B, between the grains. Then, the conductivity in the nonlinear region is given by [20]:

$$\sigma_2 = \sigma_1 \exp\left\{\frac{(\alpha-1)(E_2-E_1)}{E_2}\right\} \qquad (2)$$

where σ_1 is the conductivity in the low field region (first region). E_1 and E_2 are the applied fields across the nonlinear region. In Fig. 5 (a – c), we have presented the electrical conductivity σ against temperature through the three different regions for all the samples.

It is clear that σ increases with increasing temperature up to 500 K, in the following order: Ni $>$ Zn $>$ Fe. The lower values of conductivity at low temperature (300 K) can be understood as the consequence of the high porosity and small grain size for this type of samples. It is also related to the shape of the intergranular Schottky barrier, which is expected to be wider at low temperature. However, at high temperature up to 500 K, the Schottky barrier is supposed to be thin as a result of electrically active defects produced during heat treatments. In particular, the samples at 300 K show a faster response to the presence of oxygen vacancies, while they show a delay in their response at 500 K. The presence of these vacancies may originate due to the changes in the height and shape of the barrier and due to adsorption at intergranular regions. This behavior is consistent with the behaviors of breakdown field and nonlinear coefficient

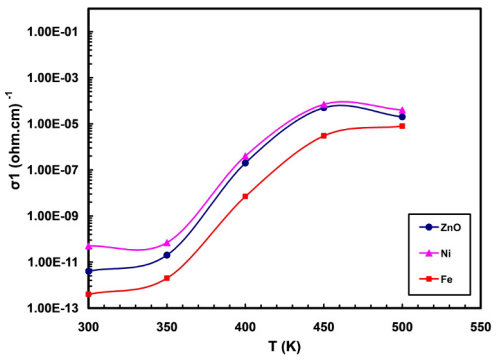

(a)

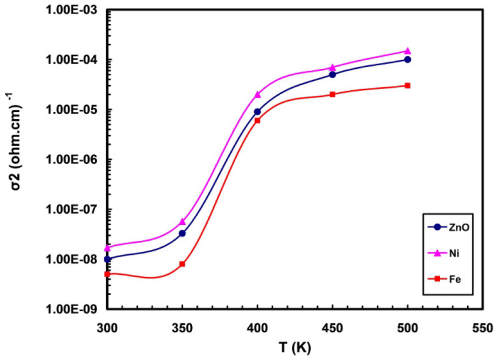

(b)

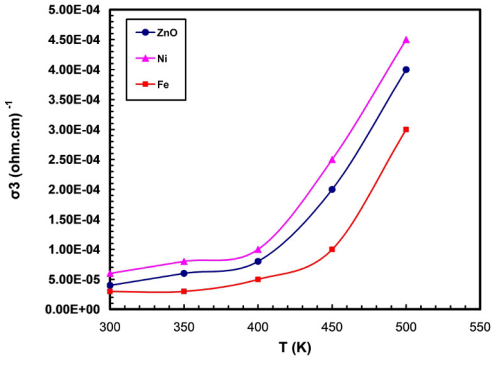

(c)

Fig. 5. Electrical conductivity versus temperature for $Zn_{0.95}M_{0.05}O$ samples (a) for the first region, (b) for the second region and (c) for the third region.

against temperature. However, the conductivity-temperature dependence is found to obey the well-known Arrhenius relation;

$$\sigma = \sigma_0 \exp\left(\frac{E_a}{K_B T}\right) \qquad (3)$$

where σ and σ_o are the electrical conductivities at temperatures T and T_o, respectively. E_a is the activation energy over the temperature range. Fig. 6 shows the variation of ln σ against reciprocal of temperature, 1000/T. It is clear that the electrical conductivity σ gradually increases as the temperature increases up to 500 K, in the following order: Ni > Zn > Fe. Anyhow, we have obtained a saturation in the conductivity curves at 300 K. By excluding this point, the activation energy can be calculated from the slope of each plot. The values of activation energies E_a, listed in Table 1, are 0.194 eV, 0.138 eV and 0.223 eV for the tested samples, in the following order: Zn, Ni and Fe. Anyhow, a lot of studies have been made on the effects of 3d transition-metal impurities on the electrical conductivity of ZnO varistor. They postulated that these metals could enhance the excess oxygen concentration in the grain boundary region and a potential barrier is formed preferentially [21–23]. Therefore, the electrical conductivity of the doped samples is apparently lower than that of the ZnO, and the grain boundary is more resistive than the grain itself. Therefore, the doping additives can be used in ZnO varistor to build up the potential barrier in the grain boundary.

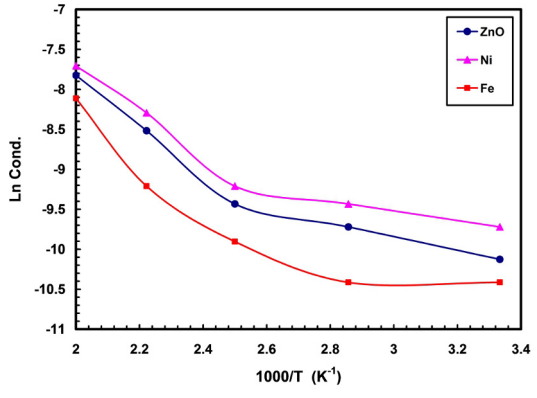

Fig. 6. ln σ versus 1000/T for $Zn_{0.95}M_{0.05}O$ samples.

Based on the present data, let us now discuss the effect of the Fe and Ni doping in place of Zn. The Fe addition to ZnO produces a large amount of pores, which may be the main reason for the significant decrease in the conductivity of the Fe doped sample. Also, the solid solution of Fe in ZnO samples may become the main factor influencing the increase in the electrical conductivity against temperature [24–26]. It is well known that the trivalent ion, dissolved in ZnO, acts as a shallow donor and is the main reason for the increase of ZnO conductivity [25, 26]. Anyhow, the obtained results of conductivities show that when Fe is dissolved in ZnO, it behaves as a deep donor and depresses the concentrations of the intrinsic donors during sintering, and consequently, the electrical conductivity at room temperature is lowered. But with increasing temperature, the Fe deep donors may start to ionize due to thermal ionization, resulting in an increase of the conductivity. Furthermore, the concentration of native defects, namely the intrinsic donor defects, increases and results in the apparent increase of the conductivity [27], inconsistent with the obtained results.

Ni^{2+} is considered to be a neutral dopant since the Ni^{2+} ions are substituted for Zn^{2+} ions in the ZnO lattice, where 2^+ of Zn is replaced by 2^+ of Ni. Therefore the potential barrier and electrical conductivity should be unaffected, which is not reflected in the results. This is because Ni is a magnetic ion with a magnetic moment of 3.2 μ_B [28]. Therefore, the potential barrier may be deformed by Ni magnetic moment, and consequently, the electrical conductivity is improved, but remains higher than that of Fe. However, the d bands result in energy of roughly 1 eV too low for activation as compared to the experimental value [29–33]. This deviation can be attributed to the measured exciton energies influenced by electronic relaxations, which are expected to be mostly pronounced for the highly localized cationic semi-core d states, inconsistent with the values of E_a deduced from the conductivity curves. However, in Schottky-type barrier, the resistivity is related to electron concentration, n in the bulk and to the barrier height, Φ_B as, $\Phi_B \alpha (\frac{n}{\Phi_B})^{\frac{1}{2}}$ [27]. A diminution in the resistivity could then be ascribed to an increase in the potential barrier height or to a decrease in the donor concentration or to both phenomena occurring simultaneously. Therefore, the effective activation energy as well as the potential barrier height is raised when the doping is incorporated to the barrier formation at the grain-grain interface. This is consistent

with the behavior of potential barrier for Fe sample rather than that of Zn and Ni samples as discussed above. So, the Ea is higher for Fe compared to Zn and Ni , as it has been obtained.

4. Conclusions

Structural and electrical properties of $Zn_{0.95}M_{0.05}O$ ceramic varistors, M = Zn, Ni and Fe is reported. We have shown that addition of doping does not influence the hexagonal wurtzite structure of ZnO ceramics, while the grain size is affected. The breakdown field is gradually decreased as the temperature increases, in the following order: Fe $>$ Zn $>$ Co. The nonlinear region is observed as the temperature increases up to 400 K, and completely disappears with further increase of temperature up to 500 K. Moreover, the electrical conductivity is gradually increased as the temperature increases up to 500 K, in the following order: Ni $>$ Zn $>$ Fe. On the other hand, the activation energies are 0.194, 0.138 and 0.223 eV for all samples, and in the following order: Fe, Zn and Ni. We believe that valence states, magnetic moment and thermo-ionic emission produced by the doping are responsible for the present behavior.

Acknowledgements

This work was supported in part from the research advancement projects no: 140082 of King Faisal University, Saudi Arabia. The authors would like to thank the Deanship of Scientific Research, KFU for providing facilities and maintenance support during the present work.

References

[1] GUPTA T.K., *J. Am. Ceram. Soc.*, 73 (1990), 1817.
[2] GLOT A.B., *J. Mater. Sci.-Mater. E.*, 17 (2006), 755.
[3] SENOS A.M.R., SANTOS M.R., MOREIRA A.P., VIEIRA J.M., In Surface and Interfaces of Ceramic Materials, ED. DUFOUR L. C., MONTY C., PETOT-ERVAS G., NATO ASI Series, Kluwer Academic, London (1988), 553.
[4] SENOS A.M.R., VIEIRA J.M., In Proceedings of the International Conference Third Euro-Ceramics, ED. DURAN P. , FERNANDEZ J. F., FAENZA EDIT RICE IBERICA FAENZA S. L., 1 (1993), 821.
[5] SENOS A.M.R., PhD Thesis, University of Aveiro, Aveiro (1993).
[6] LEVINE J.D., CRIT C.R.C., *Rev. Solid State. Sci.*, 5 (1975), 597.
[7] BERNASCONI J., STRASSLER S., KNECHT B., KLEIN H.P., MENTH A., *Solid. State. Commun.*, 21 (1977), 867.
[8] EINZINGER R., *Appl. Surf. Sci.*, 3 (1979), 390.
[9] SENOS A.M.R., BAPTISTA J.L., *J. Mat. Sci. Lett.*, 3 (1984), 213.
[10] GLOT A.B., HOGARTH C.A., BULPETT R., *Int. J. Electron.*, 65 (1988), 797.
[11] MAHAN G.D., LEVINSON L.M., PHILIPP H.R., *J. Appl. Phys.*, 50 (1979), 2799.
[12] In Proceedings of the Mater Res Soc Ann Meet., On Grain boundaries in Semiconductors, ED. BY PIKE G.E., SEAGER C.H., LEAMY H.J., Elsevier (1982), 369.
[13] KISI E., ELCOMBE M.M., *Acta Crystallogr. C*, 45 (1989), 1867.
[14] ÖZGÜRA Ü. et al., *J. Appl. Phys.*, 98 (2005), 041301.
[15] SEDKY A., ABU-ABDEEN M., ABDEL-AZAZ AL-MOULHEM, *Physica B*, 388 (2007), 266.
[16] DESHPANDE V.V., PATIL M.M., RAVI V., *Ceram. Int.*, 32 (2006), 85.
[17] HOUABES M., BERNIK S., TALHI CH., BUI A., *Ceram. Int.*, 29 (6) (2005), 783.
[18] MATSOUKA M., *Jpn. J. Appl. Phys.*, 10 (6) (1971), 736.
[19] CHOON-WOO NAHM, *Mat. Sci. Eng. B-Solid.*, 136 (2 – 3) (2007), 134.
[20] SEDKY A., E.EL-SUHEEL E., *Chin. Phys. B*, 21 (11) (2012), 116103.
[21] OHASHI N. et al., *Jpn. J. Appl. Phys.*, 38 (1999), 5028.
[22] OBA F., TANAKA I. , ADACHI H., *Jpn. J. Appl. Phys.*, 38 (1999), 3569.
[23] MANTAS P.Q., BAPTISTA J.L., *J. Eur. Ceram. Soc.*, 15 (1995), 605.
[24] HAN J., MANTAS P.Q., SENOS A.M.R., *J. Eur. Ceram. Soc.*, 21 (2001), 1883.
[25] CARLSON W.G., GUPTA T.K., *Appl. Phys.*, 53 (1982), 5746.
[26] TSAL Y.L., HUANG C.L., WEI C.C., *J. Mater. Sci. Lett.*, 4 (1985), 1305.
[27] AYMAN SAWALHA , SEDKY A., ABU-ABDEEN M., *Physica B*, 404 (2009), 1316.
[28] GUANGQING PEI, CHANGTAI XIA, SHIXUN CAO, JUNGANG ZHANG, FENG WU, JUN XU, *J. Magn. Magn. Mater.*, 302 (2) (2006), 340.
[29] WEI S. H., ZOUNGER A., *Phys. Rev. B*, 37 (1988), 8958.
[30] MARTINS J. L.,TROULLIER N., WEI S. H., *Phys. Rev. B*, 43 (1991), 2213.
[31] XU Y.N., CHING W. Y., *Phys. Rev. B*, 48 (1993), 4335.
[32] VOGEL D., KRÜGER P., POLLMANN J., *Phys. Rev. B*, 52 (1995), R14316.
[33] ZAKHAROV O., RUBIO A., BLASÉ X., COHEN M. L., LOUIE S. G., *Phys. Rev. B*, 50 (1994), 10780.

Received 2013-09-04
Accepted 2013-11-23